

Equilibrium basal-plane magnetization of superconductive $\text{YNi}_2\text{B}_2\text{C}$ - the influence of non-local electrodynamics

J.R. Thompson^{1,2}, A.V. Silhanek³, L. Civale³, K.J. Song², C.V. Tomy⁴, and D.McK. Paul⁵

¹*Oak Ridge National Laboratory, Oak Ridge, Tennessee 37831-6061.*

²*Department of Physics, University of Tennessee, Knoxville, Tennessee 37996-1200.*

³*Comisión Nacional de Energía Atómica-Centro Atómico Bariloche and Instituto Balseiro, 8400 Bariloche, Argentina.*

⁴*Department of Physics, I.I.T. Powai, Mumbai, 400076, India*

⁵*Department of Physics, University of Warwick, Coventry, CV4 7AL, United Kingdom.*

(submitted October 9, 2000; revised 22 February 2001)

For a single crystal of $\text{YNi}_2\text{B}_2\text{C}$ superconductor, the equilibrium magnetization M in the square basal plane has been studied experimentally as a function of temperature and magnetic field. While the magnetization $M(H)$ deviates from conventional London predictions, a recent extension of London theory (to include effects of non-local electrodynamics) describes the experiments accurately. The resulting superconductive parameters are well behaved. These results are compared with corresponding findings for the case with M perpendicular to the basal plane.

I. INTRODUCTION

Borocarbide superconductors continue to reveal new and interesting features.¹ This family of compounds, $\text{ReNi}_2\text{B}_2\text{C}$, exhibits superconductivity for $\text{Re} = \text{Lu}, \text{Y}, \text{Tm}, \text{Er}, \text{Ho}$ and Dy . The last four of these order antiferromagnetically below the Neel temperature T_N that ranges from 1.5 K to 10 K. The relatively high superconducting transition temperature T_c and the broad variation of the ratio T_N/T_c within the family make these materials particularly appropriate to explore the microscopic coexistence of superconductivity and localized magnetic moments.²⁻⁶

A second remarkable feature in these compounds is the formation of superconducting vortex lattices [FLL] with symmetries other than the hexagonal one.^{2,7-9} The presence of these non-hexagonal lattices has been attributed to the effects of nonlocal electrodynamics, which arise when the electronic mean free path ℓ is larger than the BCS zero temperature superconducting coherence length ξ_0 . Nonlocal electrodynamics in superconductors had been traditionally associated with very low values of the Ginzburg Landau parameter, $\kappa \sim 1$. Borocarbide superconductors have κ values in the range of 10 to 20. However, the availability of very clean single crystals with large ℓ permits the observation of nonlocal effects in these intermediate κ materials.

Nonlocality influences the equilibrium magnetic response of the vortex lattice in various ways. Song et al.¹⁰ have shown that, when the applied field \mathbf{H} is parallel to the crystallographic c -axis of a $\text{YNi}_2\text{B}_2\text{C}$ crystal, the reversible magnetization in the mixed state deviates from the logarithmic dependence on magnetic field, $M \propto \ln(H_{c2}/H)$, which is expected from the standard London model.¹¹ Such deviations could be quantitatively accounted for within the framework of a nonlocal generalization of London theory, as developed by Kogan and Gurevich.¹²

More recently, we have measured¹³ M of this compound for \mathbf{H} lying within the basal plane, and we found that it oscillates with angular periodicity $\pi/2$, a behavior that is incompatible with the standard London model. Indeed, the familiar superconductive mass anisotropy with components m_{ij} , which plays a major role in the layered high- T_c materials, is a second rank tensor. Thus, in the square ab basal plane of this tetragonal compound one has $m_{aa} = m_{bb}$, which immediately implies that the response within the plane should be isotropic. In contrast, Kogan's nonlocal scenario¹² contains a fourth rank tensor that breaks the basal plane isotropy and provides for the observed four-fold anisotropy.

In this paper we expand the analysis of the reversible magnetization of the vortex system in $\text{YNi}_2\text{B}_2\text{C}$ by presenting detailed measurements of $M(H, T)$ for \mathbf{H} in the basal plane of the crystal. Within the framework of the Kogan-Gurevich model¹², we obtain explicit expressions for the magnetization in the ab -plane by expanding the free energy appropriate for this configuration¹⁴ to first order in the basal-plane anisotropy. This approximation provides an excellent description of the experimental results and, furthermore, the resulting parameters for the superconductor are well behaved and exhibit a remarkable consistency with results from band structure calculations. These aggregate findings give unimpeachable evidence for a profound impact of nonlocal electrodynamics on clean, intermediate κ borocarbide superconductors.

II. THEORETICAL BACKGROUND

Standard local London anisotropic theory provides a simple logarithmic field dependence for the equilibrium magnetization. For intermediate fields $H_{c1} \ll H \ll H_{c2}$, one has¹¹ (for \mathbf{H} parallel to the k -th principal axis)

$$\frac{M^k}{M_0^k} = -\ln\left(\frac{\eta H_{c2}^k}{B}\right), \quad M_0^k = \frac{\Phi_0}{32\pi^2\lambda_i\lambda_j} \quad (1)$$

Here η is a constant of order unity; λ_i is the London penetration depth corresponding to screening by currents in the \mathbf{j} -direction, with $\mathbf{H} \parallel \mathbf{k}$ -axis; $H_{c2}^k = \Phi_0/2\pi\xi_i\xi_j$ is the upper critical field in the \mathbf{k} -direction, with ξ being the Ginzburg-Landau coherence length at temperature T . Experimentally, we will make the usual approximation that the flux density $B = H + 4\pi M$ can be replaced by the applied field H , since the magnetization $M \ll H$ in all cases treated here.

In the Kogan-Gurevich non-local formulation of London theory¹² there is a third independent length scale, the nonlocality radius ρ , which depends on ℓ and T and also reflects the material anisotropy. It has the form $\rho = \lambda\sqrt{n}$, where $\lambda = (\lambda_a\lambda_b\lambda_c)^{1/3}$ and n is the appropriate component of the fourth rank tensor \hat{n} , given by

$$\lambda^2 n_{ijklm} \propto \gamma(T, \ell) \langle v_i v_j v_l v_m \rangle / \langle v^2 \rangle^2. \quad (2)$$

Here \mathbf{v} is the Fermi velocity and $\langle \dots \rangle$ indicates averages over the Fermi surface. The function $\gamma(T, \ell)$, that contains all the temperature and mean free path dependencies, has been evaluated by Kogan et al.^{12,15}

When non-locality is important, the scale $H_{c2} \sim \Phi_0/\xi^2$ for M is replaced by another magnetic field scale $H_0 \sim \Phi_0/\rho^2$. As $\gamma(T, \ell)$ slowly decreases with increasing T , so does ρ , and consequently H_0 slowly increases with temperature, in contrast to H_{c2} . One consequence of the theory is that the quantity $\gamma H_0 \sim 1/\xi_0^2$ should be independent of temperature, which is a prediction that we test later.

In a tetragonal material \hat{n} has four independent components, $n_1 = n_{aaaa}$, $n_2 = n_{aabb}$, $n_3 = n_{cccc}$ and $n_4 = n_{aacc}$. For $\mathbf{H} \parallel \mathbf{c}$ -axis, the resulting expression for $M^c(H, T)$ is¹²

$$\frac{M^c}{M_0^c} = -\ln\left(\frac{H_0^c}{B} + 1\right) - \frac{H_0^c}{(H_0^c + B)} + \zeta^c \quad (3)$$

where $M_0^c = \Phi_0/32\pi^2\lambda_{ab}^2$, $H_0^c = \Phi_0/4\pi^2\lambda^2 n_2$ (for a square FLL), and $\zeta^c(T) = \eta_1 - \ln(H_0^c/\eta_2 H_{c2}^c + 1)$, with both η_1 and η_2 constants of order unity.

If \mathbf{H} lies in the ab -plane the analysis is more complex. In a previous study,¹³ we described the basal plane anisotropy in M by assuming the validity of an expression analogous to Eq. (3) and proposing a four-fold oscillation in H_0 . The empirical expression so obtained successfully captured the basic features of the in-plane magnetic response, but the link between the amplitude of the oscillations and the more fundamental material parameters was undefined.

According to a subsequent generalization of the formalism, developed¹⁴ for the case of \mathbf{H} in the ab -plane, the free energy is approximately given by

$$F = M_0^{ab} B \int_{u_1}^{u_2} \frac{du}{\sqrt{(u+n_4)(u+n_4+d(\varphi)/4)}} \quad (4)$$

Here $M_0^{ab} = \Phi_0/32\pi^2\lambda_{ab}\lambda_c$, $u_1 = (4\pi^2\kappa^2)^{-1}$ and $u_2 = 2\pi u_1(H_{c2}/B)$. (Within this approximation, the very small anisotropy¹⁶ in H_{c2} can be ignored.) Equation (4) holds whenever $u \ll 1$, so that terms of order u^2 can be neglected. For $\text{YNi}_2\text{B}_2\text{C}$ we have $\kappa \sim 10$, thus $u_1 \sim 2.5 \times 10^{-4}$ and $u_2 \sim 1.6 \times 10^{-3} H_{c2}/B$. In our analysis of the basal-plane magnetization, $(H_{c2}/B) \leq 40$ in all cases (see section IV) thus $u_2 \leq 0.05$ and the approximation is valid.

The in-plane anisotropy is accounted for by $d(\varphi)$,

$$d = n_3\Gamma^2 + \frac{n_1}{\Gamma^2} - 6n_4 - \frac{n_1 - 3n_2}{2\Gamma^2} \sin^2(2\varphi) \quad (5)$$

where $\Gamma^2 = m_c/m_a$ is the usual mass anisotropy between the a and c -axes, and φ is the angle between the vortices and the a -axis. If $d = 0$ the in-plane response would be isotropic and integration of Eq. (4) would result in a magnetization $M = -\partial F/\partial B$ identical to Eq. (3). However, for $d \neq 0$ the in-plane magnetization cannot in general be reduced¹⁴ to the form (3).

The integrand of (4) can be expanded in powers of the variable $d(\varphi)/4(u+n_4)$ and integrated term by term. The resulting series can be differentiated with respect to B to obtain M^{ab} . The leading term, M_{iso}^{ab} , is independent of d and represents a large contribution to the magnetization that is isotropic within the plane

$$\frac{M_{iso}^{ab}}{M_0^{ab}} = -\ln\left(\frac{H_0^{ab}}{B} + 1\right) - \frac{H_0^{ab}}{(H_0^{ab} + B)} + \zeta^{ab} \quad (6)$$

where $H_0^{ab} = \Phi_0/4\pi^2\lambda^2 n_4$ (Also in this case, the numerical factors are valid for a square FLL). The term ζ^{ab} arises from the core contribution to the free energy (not included in Eq. (4)); it is analogous to ζ^c in both form and origin, as described previously.^{12,14} Eq. (6) has the same functional form as Eq. (3), but the anisotropy between the c -axis and the plane is reflected in both the prefactor M_0 and the field scale H_0 .

The second term in the expansion, M_1^{ab} , is linear in $d(\varphi)$ and accounts for the in-plane fourfold anisotropy in M^{ab} to leading order:

$$\frac{M_1^{ab}}{M_0^{ab}} = -\frac{d}{8n_4} \frac{B}{B + H_0^{ab}} \left[\frac{H_0^{ab}}{H_0^{ab} + B} - \frac{\frac{H_{c2}}{B} - 1}{\left(\frac{H_{c2}}{H_0^{ab}} + 1\right)} \right] \quad (7)$$

In the above scenario H_{c2} tends toward zero as $T \rightarrow T_c$, while H_0 increases with temperature. These differing temperature dependencies mean that for clean materials, the non-local expressions Eqs. 3 and 6 reduce to the local form, Eq. 1, as T approaches T_c , while M_1^{ab} from Eq. 7 vanishes. Thus, the non-local theory predicts that the equilibrium magnetization in a clean sample should vary logarithmically with field near T_c , but deviate progressively from logarithmic behavior at low temperatures. Furthermore, as materials become dirtier so that ρ becomes shorter and H_0 increases, the non-local expressions reduce to the local form *at all temperatures*.

Our purpose is to analyze the in-plane magnetization using Eqs. 6 and 7. We thus need to estimate the importance of the various terms in the expansion. According to electron band calculations,¹⁷ for $\text{YNi}_2\text{B}_2\text{C}$ we have

$$\begin{aligned}
\langle v^2 \rangle &= 1.50 \times 10^{15} (\text{cm}/\text{sec})^2 \\
\langle v_a^2 \rangle &= 0.87 \times 10^{15} (\text{cm}/\text{sec})^2 \\
\langle v_c^2 \rangle &= 0.85 \times 10^{15} (\text{cm}/\text{sec})^2 \\
\langle v_a^4 \rangle &= 1.15 \times 10^{30} (\text{cm}/\text{sec})^4 \\
\langle v_a^2 v_b^2 \rangle &= 1.75 \times 10^{29} (\text{cm}/\text{sec})^4 \\
\langle v_c^4 \rangle &= 7.71 \times 10^{29} (\text{cm}/\text{sec})^4 \\
\langle v_a^2 v_c^2 \rangle &= 2.41 \times 10^{29} (\text{cm}/\text{sec})^4
\end{aligned} \tag{8}$$

Based on those values we can calculate the relations between all the components of \hat{n} using Eq. (2). In section IV we will compare these band calculation estimates with our experimental results. In particular, we are interested in the dimensionless prefactor $d/8n_4$ that sets the order of magnitude in Eq. 7. It is also useful to split d in two parts, $d = d_1 + d_2 \sin^2(2\varphi)$. Using Eq. 5 we obtain

$$\frac{d_1}{8n_4} \approx 0.23 \quad \frac{d_2}{8n_4} \approx -0.13 \tag{9}$$

In section IV we will make use of these estimates to gain an idea of the goodness of our approximations. For comparison, we can calculate the equivalent values for the similar material $\text{LuNi}_2\text{B}_2\text{C}$, using the Fermi-surface averages given previously.¹⁸ The results are $d_1/8n_4 \approx 0.42$ and $d_2/8n_4 \approx -0.20$. The larger values for the Lu-based system mean that the first-order expansion in Eqs. 6-7 is more accurate for the yttrium-based compound, while the amplitude of oscillation in the basal plane magnetization can be larger for $\text{LuNi}_2\text{B}_2\text{C}$.

III. EXPERIMENTAL ASPECTS

The $\text{YNi}_2\text{B}_2\text{C}$ single crystal was grown by a high temperature flux method using Ni_2B flux, using isotopic ^{11}B to reduce neutron absorption in complementary scattering studies. The 17 mg crystal is the same as that used in previous investigations by Song et al.¹⁰ and Civale et al.¹³ It is a slab of thickness $t \sim 0.5\text{mm}$ in the c -axis direction, with a mosaic spread of less than 0.2° , as determined by neutron diffraction. In the basal plane the shape is approximately elliptical with principal axes of length ~ 2.0 and 2.5mm , which approximately coincide with the two equivalent (110) axes of the tetragonal structure.

Magnetic studies were conducted in a SQUID-based magnetometer Quantum Design MPMS-7 equipped with a compensated 70 kOe magnet. Normally, scan lengths of 3cm were used. The crystal was glued onto a thin Si-disk and mounted in a Mylar tube for measurement with the magnetic field \mathbf{H} applied in the basal plane, along either the [100] or the [110] axis, with an accuracy better than

3° . For both orientations, the magnetization \mathbf{M} is parallel to \mathbf{H} by symmetry, thus only the longitudinal component measured by the magnetometer needs to be considered. This is also true with $\mathbf{H} \parallel [001]$, as was the case for the previous data that will be included in our analysis. Then, from now on we will ignore the vector nature of \mathbf{M} and denote it simply as M . The diamagnetic moment of the addenda (silicon disk plus glue), which was measured separately, was linear in H , isotropic, and non-hysteretic. This signal, $m_{Si} = (-5.4 \times 10^{-9} \text{emu/Oe})H$, was always small compared with the moment of the crystal, and was subtracted from all the data prior to any further analysis.

In the mixed state, hysteresis loops $M(H, T)$ were measured. The maximum H was 65kOe in all cases. Measurements were also conducted in the normal state at temperatures up to 300K , in order to correct for the normal state background moment. It is worth noting that the magnetization is small, compared to the applied field, in all cases considered here. Thus demagnetizing effects are negligible: for $\mathbf{H} \parallel ab$ -plane, we obtain from the Meissner state response¹³ that the effective demagnetization factor $D \approx 0.1$. Then in the mixed state, the effective field $H_{eff} = H_{applied} - 4\pi DM$ differs from the applied field by less than 1 % is the worst case and we need to consider only the magnetizing field "H." Furthermore, for comparison with theoretical expressions, we can approximate the flux density $B = H + 4\pi M$ by H with an accuracy of a few percent and generally better.

The superconductive transition temperature, measured in a small applied field, was $T_c = 14.5\text{K}$. Measurement of the electrical resistivity using a van der Pauw method gave an electrical resistivity of $4\mu\Omega - \text{cm}$ at 20K and a residual resistance ratio of 10, yielding an electronic mean free path $\ell \approx 300 \text{Å}$. Using this and values of H_{c2} (for $H \parallel c$ -axis), Song et al. deduced the values $\xi_0 = 120 \text{Å}$ for the BCS coherence length at $T = 0$ and $\kappa \sim 10$. Other superconducting parameters for this compound are collected in Table I.

IV. RESULTS AND DISCUSSION

For magnetic field orientations $\mathbf{H} \parallel [100]$ and $\mathbf{H} \parallel [110]$, we measured isothermal magnetization loops $M(H)$ at temperatures $T = 3$ to 14K , in 1K intervals, and also at 18K , slightly above T_c . Three of those loops, with $\mathbf{H} \parallel [110]$, are shown in Fig. 1, at temperatures $T = 5\text{K}$, 12K and 18K , i.e., well below, near, and just above T_c . The magnetic response of this material in the superconducting mixed phase is slightly irreversible, reflecting weak pinning of flux lines. Now, as the only source of magnetic hysteresis is vortex pinning, $M(H)$ becomes reversible for $H > H_{c2}(T)$. Based on the Bean's critical state model, we calculated the equilibrium magnetization as the average $M_{eq}(H) = [M^\uparrow + M^\downarrow]/2$ of the magnetization values measured in the field-increasing and field-decreasing branches of the loop, respectively.

The result for $T = 5K$ is shown as a dashed line in Fig. 1. The identification of $M_{eq}(H)$ with the average between the branches of the loop increases in accuracy as the width of the hysteresis loop $[M^\uparrow - M^\downarrow]$ decreases. For each temperature, we disregard the low field data where large hysteresis introduces a significant uncertainty in the determination of M_{eq} . Experimentally, as the field decreases, the width of the $M(H)$ loop increases continuously and smoothly. Then at some temperature-dependent low field, M changes abruptly as it reaches a minimum and starts to increase. This feature is visible in Fig. 1 for $T = 5$ and 12 K, for example. Below this field, the hysteresis grows suddenly. We compute the average magnetization starting at a field slightly above this minimum.

It is apparent in Fig. 1 that the magnetization M_{eq} does not vanish above H_{c2} and above T_c . This indicates the presence of a normal state contribution $M_{ns}(H, T)$ to the magnetization (recalling that the signal from the sample holder has been already subtracted). Pure $\text{YNi}_2\text{B}_2\text{C}$ has no localized moments, thus in the normal state it is expected to exhibit a linear and nominally temperature-independent paramagnetic (Pauli and Van-Vleck) susceptibility χ_0 . However, close inspection of the data indicates that this intrinsic term cannot account for the entire normal state signal. Indeed, $M_{ns}(H, T)$ is not linear in H and it grows as T decreases, thus pointing to the presence of localized moments. The small magnitude of the signal suggests, on the other hand, that this contribution arises from magnetic impurities. To confirm this, we measured the temperature dependence of $M_{ns}(H, T)$ from $16K$ to $300K$ at several fixed fields. The results for $H = 1$ and $5kOe$ are shown in the inset of Fig. 1. As the localized moments are very dilute, no magnetically ordered phase should appear and one can expect a Curie Law dependence. The solid lines in the inset are fits to $M_{ns}/H = [\chi_0 + C/T]$. The Curie term corresponds to a rare earth impurity content of ~ 0.1 at % relative to yttrium, most likely contaminants in the yttrium starting material.

To isolate the magnetization associated with the vortex state, it is necessary to remove the paramagnetic background. The normal state magnetization M_{ns} is well described by the expression

$$M_{ns} = \chi_0 H + M_{sat} B_J \left(\frac{g\mu_B J H}{k_B T} \right) \quad (10)$$

where χ_0 is the temperature independent susceptibility obtained as explained above and B_J is the Brillouin function for effective angular momentum J . For small values of the argument H/T , the Brillouin function leads to the Curie susceptibility, of course.

The magnetic signal arising from the localized moments is clearly observed in Fig. 2, where $[M_{eq} - \chi_0 H]$ is plotted as a function of H/T . The figure includes experimental data from temperature sweeps at three values of H , and from isothermal loops at temperatures down to

$5K$. At each T , the onset of the superconducting signal below $H_{c2}(T)$ is clearly observed in the nearly vertical trace of data below the envelope curve. It is also apparent that for $H > H_{c2}(T)$ all the data at different T overlap on a single curve arising from the paramagnetic contribution of the magnetic impurities. The solid line is a nonlinear fit to Eq. 10 that yields parameter values $J = 3/2$ and $g = 6$. The saturation magnetization $M_{sat} = 0.92G$ corresponds to $\sim 7 \times 10^{-4}$ per formula unit content of rare earth impurities, most likely trace contaminants in the yttrium starting material. At this concentration, the magnetic impurity ions are isolated, but strongly influenced by the crystal field of the host, producing an anisotropic magnetic response in the normal state. The susceptibility is smaller for $H \parallel c$ -axis, as found for $\text{ReNi}_2\text{B}_2\text{C}$ crystals with $\text{Re} = \text{Tb}, \text{Dy},$ and Ho , but not Tm .²⁰ These qualitative similarities show that (a mixture of) any of several rare earth impurities can generate the observed paramagnetic response. The central and important point here, however, is that the empirical fit to Eq. 10 provides a precise description of the normal state signal, so that the superconductive magnetization can be isolated for analysis.

The resulting (background-corrected) superconducting state equilibrium magnetization $M = M_{eq} - M_{ns}$ is shown in Fig. 3, as a function of magnetic field H applied along the $[110]$ axis of the crystal. Results are shown for temperatures $3K \leq T \leq 14K$ in intervals of $1K$. Qualitatively, the curves for temperatures near T_c are linear, showing the dependence on $\ln(B)$ as predicted by traditional local London theory. At lower temperatures, however, the increasing curvature visibly signals a progressive departure from local London behavior.

For a quantitative analysis, we fit the low temperature data to the non-local relation, Eq. (6), varying the parameters M_0^{ab} , H_0^{ab} , and ζ^{ab} . These fits describe the low temperature experiments very well, as shown by the solid lines in Fig. 3. The resulting values of M_0^{ab} , H_0^{ab} , and ζ^{ab} as a function of T (up to $T = 10K$) are shown in Figs. 4(a), (b) and (c) respectively. At higher temperatures, $T \geq 11K$, the system closely approximates local London behavior, with $M \propto \ln(B)$ and we analyze these data using the local expression Eq. (1). Numerically, the data close to T_c have a very shallow minimum as a function of H_0 and it becomes meaningless to fit an (essentially) straight line with three parameters. The fits to the local London relation are shown in Fig. 3 as dashed lines, and the values of $M_0(T)$ obtained by this procedure are also included in Fig. 4(a) (open symbols). In the non-local analysis, H_{c2} was not a fitting parameter. It was determined independently, as explained below.

Before we discuss the results shown in Fig. 4, we must analyze what is the error involved in taking $M^{ab} \approx M_{iso}^{ab}$, disregarding terms of higher order. To estimate the contribution M_1^{ab} given by Eq. 7, we must rely on the numerical values (9) obtained from band calculations. We see that, if at least the *signs* in (9) are correct, M_1^{ab} minimizes for $\varphi = 45^\circ$. For that reason we chose to apply Eq. 6 to

the [110] data and not to the [100] orientation. Numerically, we have $d(\varphi = 45^\circ)/8n_4 = (d_1 + d_2)/8n_4 \approx 0.10$. Thus, Eqs. (6) and (7) indicate that $M_1^{ab} \ll M_{iso}^{ab}$ over most of the field range (for instance, at $T = 3K$ and $B = 2kG$, $M_1^{ab}/M_{iso}^{ab} \sim 0.02$, and the same ratio is obtained for 6K and 10kG). We can also compare the logarithmic field derivatives of M , which give the slopes in Fig. 3. For $B \ll H_0$, to leading order we obtain $\partial M_{iso}^{ab}/\partial \ln B \approx M_0^{ab}$ and $\partial M_1^{ab}/\partial \ln B \approx 0.10(2B/H_0)M_0^{ab}$, thus for $B = 2kG$ the error in the slope produced by disregarding the second term in the expansion is less than 0.5%.

The above estimates indicate that by using Eq. (6) to analyze the magnetization in the [110] direction we are introducing an error in the determination of M_0^{ab} and H_0^{ab} of at most a few percent, which is less than the experimental noise observed in Figs. 4(a) and (b). So, it is meaningful to discuss the results shown in Fig. 4. For comparison, the corresponding results for the case¹⁰ with $\mathbf{H} \parallel [001]$ are included, too.

Figure 4(a) shows that M_0 varies linearly with T near T_c and extrapolates to zero at T_c , consistent with Ginzburg-Landau theory. From Eq. (1), the ratio $M_0^c/M_0^{ab} = \lambda_c/\lambda_{ab} = \sqrt{(m_c/m_{ab})} = \Gamma$. As expected, we find that this ratio is rather independent of temperature, $\Gamma = 1.13 \pm 0.02$. This result is very comparable with the experimental value of 1.16 for LuNi₂B₂C obtained by Metlushko et al.¹⁹ This experimental value can also be compared with the band structure calculation, since $\Gamma = \sqrt{(\langle v_a^2 \rangle / \langle v_c^2 \rangle)}$. The resulting value, 1.01, is much smaller than that deduced experimentally. Returning to the experimentally determined parameters, we can also calculate $\lambda_c(T)$, $\lambda_{ab}(T)$ and $\lambda(T)$. The results at $T = 3K$ are shown in Table 1.

The next frame, Fig. 4(b), shows $H_0(T)$. Qualitatively, H_0 for both orientations is constant at low temperature, then increases as T increases, consistent with the theoretically predicted behavior.^{12,15} In section II above, we noted that the non-local theory predicts that the quantity $H_0\gamma$ should be independent of temperature. Previously¹⁰ we found that $\xi_0 = 12$ nm; this value agrees within experimental error with that calculated from the BCS expression $\xi_0 = \hbar\langle v_F \rangle / (\pi^2 e^{-\gamma} k_B T_c) = 11.6$ nm, using $\langle v_F \rangle = 3.87 \times 10^7$ cm/sec from band structure,¹⁷ with $e^\gamma \approx 1.78$. Also, from the electrical resistivity, we have that $\ell \approx 30$ nm for this crystal and therefore evaluate the impurity parameter $\gamma(T)$ with $\xi_0/\ell = 0.3$. The results for $H_0\gamma$ are shown as open symbols in Fig. 4b, for the two orientations of magnetic field. The constancy of the product provides further solid evidence that non-local electrodynamics strongly modify the superconductive properties of clean borocarbides. From the H_0 data we can extract the nonlocality radius in both orientations, $\rho_{ab}(T) = (\Phi_0/4\pi^2 H_0^c)^{1/2}$ (see Song et al.¹⁰), and analogous expression for $\rho_c(T)$. We can also calculate two of the four independent components of the tensor \hat{n} , namely $n_2 = (\rho_{ab}/\lambda)^2$ and $n_4 = (\rho_c/\lambda)^2$. All the numer-

ical values for $T = 3K$ are listed in Table 1.

Figure 4(c) shows the temperature dependence of the fitting parameter ζ . Qualitatively, the data reflects the fact that $\zeta \sim -\ln(H_0/H_{c2})$. As T increases, H_0/H_{c2} varies little at low temperatures, but then becomes larger, due to the differing dependencies of $H_0(T)$ and $H_{c2}(T)$, thus $\zeta(T)$ decreases.

The last frame, Fig. 4d, shows $H_{c2}(T)$ in both orientations, obtained (a) by extrapolating the isothermal magnetization in the superconductive state to $M = 0$ and (b) by locating the field at which the magnetic hysteresis disappears. These results were introduced as fixed parameters in Eq. (6), as already mentioned. It is evident that $H_{c2}(T)$ curves upward near T_c . This differs from simple Ginzburg-Landau behavior, but is consistent with other observations on this material.^{21,22} Also, little anisotropy is evident between the c-axis and the basal plane values. The mass anisotropy obtained from the M_0 data (Fig. 4(a)) would imply an experimentally resolvable difference in H_{c2} . Previously, Johnson-Halperin et al.¹⁶ also found a nearly isotropic response in single crystal YNi₂B₂C. The reason for the discrepancy between the anisotropy derived from M_0 and H_{c2} remains unclear. Interestingly, LuNi₂B₂C, an isostructural, non-magnetic borocarbide superconductor with similar T_c , exhibits greater anisotropy in H_{c2} , both from the c-axis and within the basal plane.¹⁹

Next we consider the anisotropy of the magnetization within the basal plane. We have previously shown¹³ that this quantity exhibits a four-fold periodicity, which cannot be accounted for within the local London theory. In Fig. 5 we show the amplitude of the oscillation in basal plane magnetization, $\delta M = M[110] - M[100]$, as a function of field H . The experimental data for $T = 7K$ are reproduced from Civale et al.¹³, where details of the experimental procedure and data analysis are provided. Here we analyze these data using Eq. (7), where only the second term, proportional to d_2 , contributes to the oscillatory behavior. In this expression, we have already values for H_{c2} and H_0^{ab} , so there is a single unknown, $d_2/8n_4$, available for fitting the data. The result is shown as a solid line in Fig. 5. The value of the sole fitting parameter is $d_2/8n_4 = -0.136$, which we discuss below.

Let us now summarize the experimentally determined parameters related to the material anisotropy. Theoretically, five independent parameters (n_1, n_2, n_3, n_4 and Γ) are necessary to describe fully the angularly dependencies. Experimentally we have obtained three of these quantities, n_2, n_4 and Γ , plus the combination $d_2/8n_4$ that allows us to obtain the value for n_1 using Eq. 5. Thus, we have obtained four out of the five independent parameters, as shown in Table I. For comparison with band structure calculations and to eliminate poorly known prefactors, it is convenient to consider ratios relative to n_4 , as shown in Table II. The experimental and calculated ratios agree within $\sim 15\%$, which is quite reasonable given the approximations. Lastly we consider the sole fitting parameter $d_2/8n_4 \sim -0.14$ that deter-

mines the amplitude of the oscillations of M in the basal plane. This quantity has the correct sign and it lies in remarkable numerical agreement with the band structure value, -0.13 . The excellent description of the data, using parameter values measured independently here (M_0 , H_{c2} , and H_0) and with $d_2/8n_4$ almost coinciding with the calculated value, gives considerable confidence in the fundamental correctness of the non-local description.

V. CONCLUSIONS

We have measured the equilibrium magnetization in the basal plane of clean, superconducting $\text{YNi}_2\text{B}_2\text{C}$, taking careful account of background effects. Influences of non-local electrodynamics are very evident well below T_c , with the effects becoming washed out at higher temperatures as expected. The magnetic-field-dependence of the magnetization and its oscillation amplitude are well described by a generalization of London theory to include non-local influences. The results of this analysis have been compared with a corresponding study of the c -axis magnetization, thereby providing the value $\Gamma = 1.13$ for the mass anisotropy of this material. Furthermore, the experimental values for the material parameters agree overall very well with those deduced from the band structure. In summary, these clean, non-magnetic borocarbide superconductors display a rich variety of physical phenomena, requiring both 2-nd and especially 4-th rank tensors to describe their macroscopic vortex state properties.

VI. ACKNOWLEDGEMENTS

We wish to acknowledge useful discussions with V.G. Kogan, M. Yethiraj and D. K. Christen and to thank W.E. Pickett for his unpublished band structure results. A portion of the work of JRT was supported by the Science Alliance at The University of Tennessee, Knoxville. Research at ORNL was sponsored by the U.S. Department of Energy under contract DE-AC05-00OR22725 with the Oak Ridge National Laboratory, managed by UT-Battelle, LLC. Research at CAB-IB was partially supported by ANPCyT, Argentina, PICT 97 No. 01120, and by CONICET, Argentina, PIP No. 4207. A.V.S. would like to thank the CONICET for financial support.

VII. REFERENCES

- ¹ P.C. Canfield, P.L. Gammel and D.J. Bishop, *Physics Today* **51**, 40 (1998).
- ² U. Yaron, P.L. Gammel, A.P. Ramirez, D.A. Huse, D.J. Bishop, A.I. Goldman, C. Stassis, P.C. Canfield, K. Mortensen, and M.R. Eskildsen, *Nature* **382**, 236 (1996).
- ³ H. Eisaki, H. Takagi, R. J. Cava, B. Batlogg, J. J. Krajewski, W. F. Peck, Jr., K. Mizuhashi, J. O. Lee, and S. Uchida, *Phys. Rev. B* **50**, 647 (1994).
- ⁴ M. R. Eskildsen; K. Harada; P. L. Gammel; A. B. Abrahamsen; N. H. Andersen; G. Ernst; A. P. Ramirez; D. J. Bishop, K. Mortensen, D. G. Naugle, K. D. D. Rathnayaka, and P. C. Canfield, *Nature* **393**, 242 (1998).
- ⁵ P. L. Gammel, B. P. Barber, A. P. Ramirez, C. M. Varma, D. J. Bishop, P. C. Canfield V. G. Kogan, M. R. Eskildsen, N. H. Andersen, K. Mortensen, and K. Harada, *Phys. Rev. Lett.* **82**, 1756 (1999).
- ⁶ K. Nørgaard, M. R. Eskildsen, and N. H. Andersen, J. Jensen, P. Hedegård, and S. N. Klausen, and P. C. Canfield, *Phys. Rev. Lett.* **84**, 4982 (2000).
- ⁷ M. Yethiraj, D.McK. Paul, C.V. Tomy and E.M. Forgan, *Phys. Rev. Lett.* **78**, 4849 (1997).
- ⁸ Y. De Wilde, M. Iavarone, U. Welp, V. Metlushko, A.E. Koshelev, I. Aranson, G.W. Crabtree and P.C. Canfield, *Phys. Rev. Lett.* **78**, 4273 (1997).
- ⁹ D.McK. Paul, C.V. Tomy, C.M. Aegerter, R. Cubitt, S.H. Lloyd, E.M. Forgan, S.L. Lee and M. Yethiraj, *Phys. Rev. Lett.* **80**, 1517 (1998).
- ¹⁰ K.J. Song, J.R. Thompson, M.Yethiraj, D.K. Christen, C.V. Tomy and D. McK. Paul, *Phys. Rev. B* **59**, R6620 (1999).
- ¹¹ V.G. Kogan, M.M. Fang, and S. Mitra, *Phys. Rev. B* **38**, 11958 (1988).
- ¹² V.G. Kogan, A. Gurevich, J.H. Cho, D.C. Johnston, Ming Xu, J.R. Thompson and A. Martynovich, *Phys. Rev. B* **54**, 12386 (1996).
- ¹³ L. Civale, A.V. Silhanek, J.R. Thompson, K.J. Song, C.V. Tomy and D.McK. Paul, *Phys. Rev. Lett.* **83**, 3920 (1999).
- ¹⁴ V.G. Kogan, S.L. Bud'ko, P.C. Canfield and P. Miranovic, *Phys. Rev. B* **60**, R12577 (1999).
- ¹⁵ V. G. Kogan, P. Miranovic, and D. McK. Paul, in *The Superconducting State in Magnetic Fields: Special Topics and Trends*, edited by C. A. R. Sa de Melo, Directions in Condensed Matter Physics, vol **13** (World Scientific, Singapore, 1998).
- ¹⁶ E. Johnston-Halperin, J. Fiedler, D. E. Farrell, Ming Xu, B. K. Cho, P. C. Canfield, D. K. Finnemore, and D. C. Johnston, *Phys. Rev. B* **51**, 12852 (1995).
- ¹⁷ W.E. Pickett (unpublished).
- ¹⁸ V.G. Kogan, M. Bullock, B. Harmon, P. Miranović, Lj. Dobrosavljević-Grujić, P.L. Gammel, and D.J. Bishop, *Phys. Rev. B* **55**, R8693 (1997).
- ¹⁹ V. Metlushko, U. Welp, A. Koshelev, I. Aranson, G. W. Crabtree, and P. C. Canfield, *Phys. Rev. Lett.* **79**, 1738 (1997).
- ²⁰ B. K. Cho, *Physica C* **298**, 305 (1998).
- ²¹ S. V. Shulga, S. -L. Drechsler, G. Fuchs, K. H. Mueller, K. Winzer, M. Heinecke, and K. Krug, *Phys. Rev. Lett.* **80**, 1730 (1998).
- ²² G. Hilscher and H. Michor in *Studies of High Temperature Superconductors*, vol. **28**, edited by A. V. Narlikar (Nova,

TABLE I. Superconducting parameters

$\lambda = 950\text{\AA}$	$\Gamma = 1.13 \pm 0.02$
$\lambda_{ab} = 990\text{\AA}$	$\lambda_c = 880\text{\AA}$
$\rho_{ab} = 31.4\text{\AA}$	$\rho_c = 34.4\text{\AA}$
$n_1 = 6.95 \cdot 10^{-3}$	$n_2 = 1.04 \cdot 10^{-3}$
$n_3 = -$	$n_4 = 1.25 \cdot 10^{-3}$

TABLE II. Average Fermi velocities

	exp.	band calc.
n_1/n_4	5.56	4.78
n_2/n_4	0.83	0.73
n_3/n_4	-	3.2

Figure captions

Fig. 1. The magnetization of single crystal $\text{YNi}_2\text{B}_2\text{C}$ at three temperatures, with magnetic field in the basal plane, $\mathbf{H} \parallel [110]$ axis. The figure illustrates the limited irreversibility in the superconductive state below $T_c = 14.5\text{K}$, and a paramagnetic background in the normal state. Inset: Curie analysis of the normal state susceptibility in the temperature range $T = 18 - 300\text{K}$.

Fig. 2. Total equilibrium magnetization M_{eq} minus $\chi_0 H$ (see text) versus H/T obtained from isothermal field sweeps at several T and from temperature sweeps at three values of H , as indicated in the figure. The solid line is a Brillouin function (Eq. 10) fitted to the paramagnetic impurity-background data. The nearly vertical traces of data show the entry into the superconductive state.

Fig. 3. The equilibrium magnetization M_{eq} in the superconductive state with $H \parallel [110]$ axis, plotted versus H (logarithmic axis). Discrete symbols are data measured at temperatures of 14, 13, 12, ..., 3 K; straight (dashed) lines show conventional, local London behavior near T_c . A nonlocal generalization of London theory (Eq. 6, solid lines) accounts well for the pronounced deviations from local behavior at lower temperatures.

Fig. 4. Superconductive parameters of $\text{YNi}_2\text{B}_2\text{C}$ with magnetic field $H \parallel [001]$ or $H \parallel [110]$. (a) The magnitude of the equilibrium magnetization M_0 , where solid symbols denote results from the non-local analysis and open symbols come from a conventional London analysis. (b) The field scale H_0 and the (theoretically constant) quantity $H_0\gamma$ (where $\gamma = \text{impurity parameter}$; see text). (c) The fitting parameter ζ . (d) Estimates of the upper critical field H_{c2} .

Fig. 5. Amplitude of the oscillation in basal plane magnetization, $\delta M = M[110] - M[100]$, plotted versus H on a logarithmic axis. Solid line shows a fit to the oscillatory term in Eq. 7, with $H_0^{ab} = 48\text{ kOe}$ and $H_{c2}^{ab} = 33\text{ kOe}$; see text.

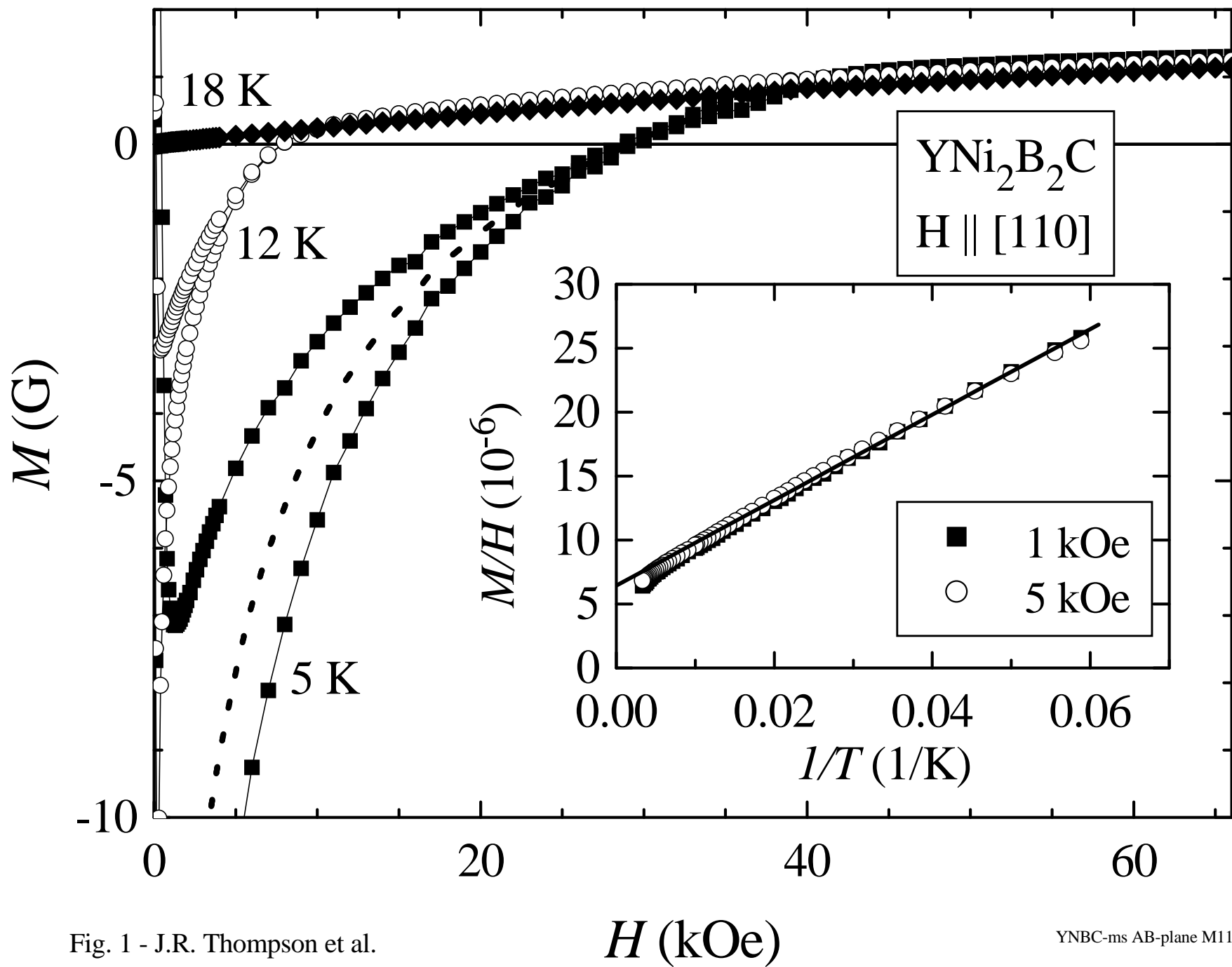


Fig. 1 - J.R. Thompson et al.

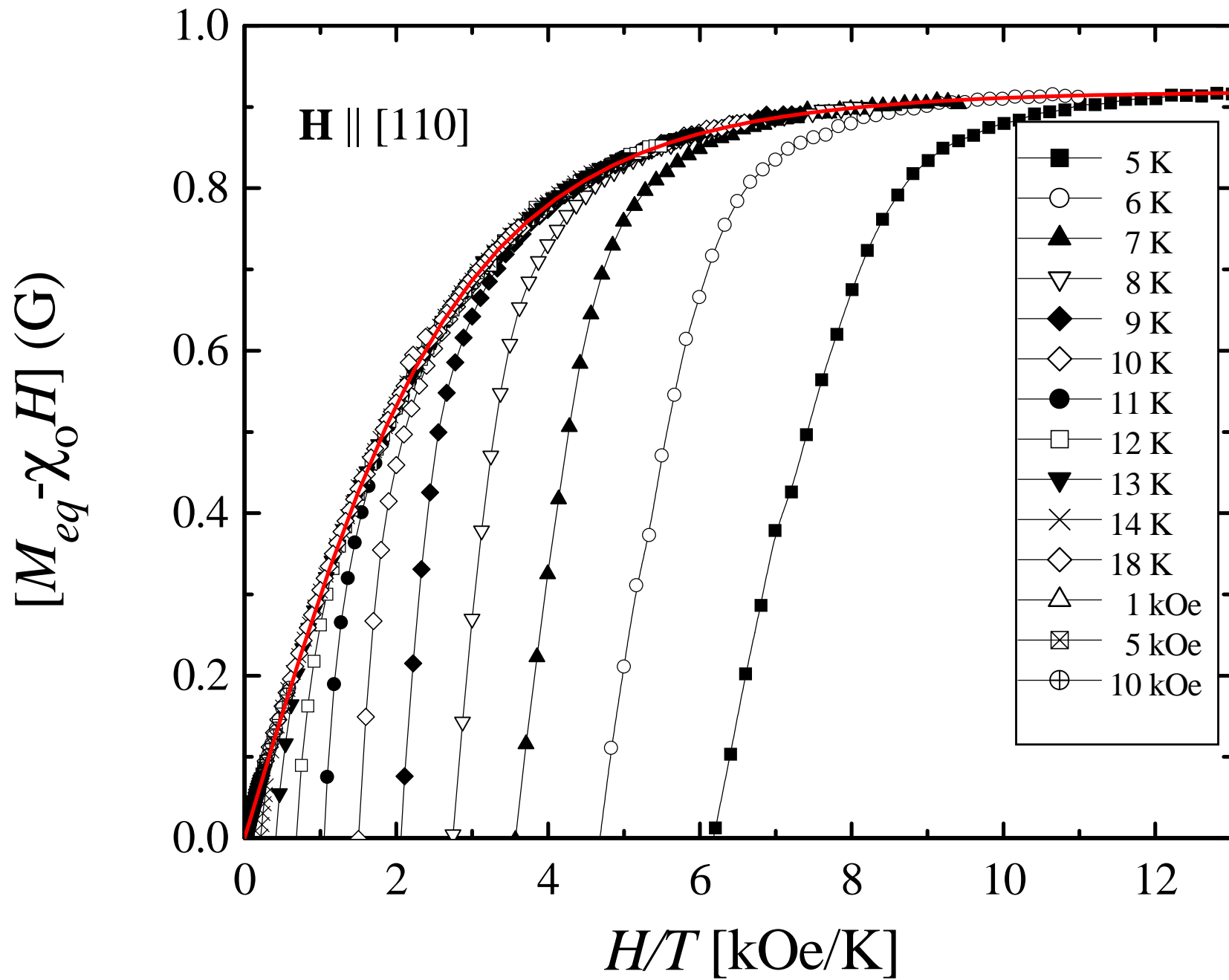


Fig. 2 - J.R. Thompson et al.

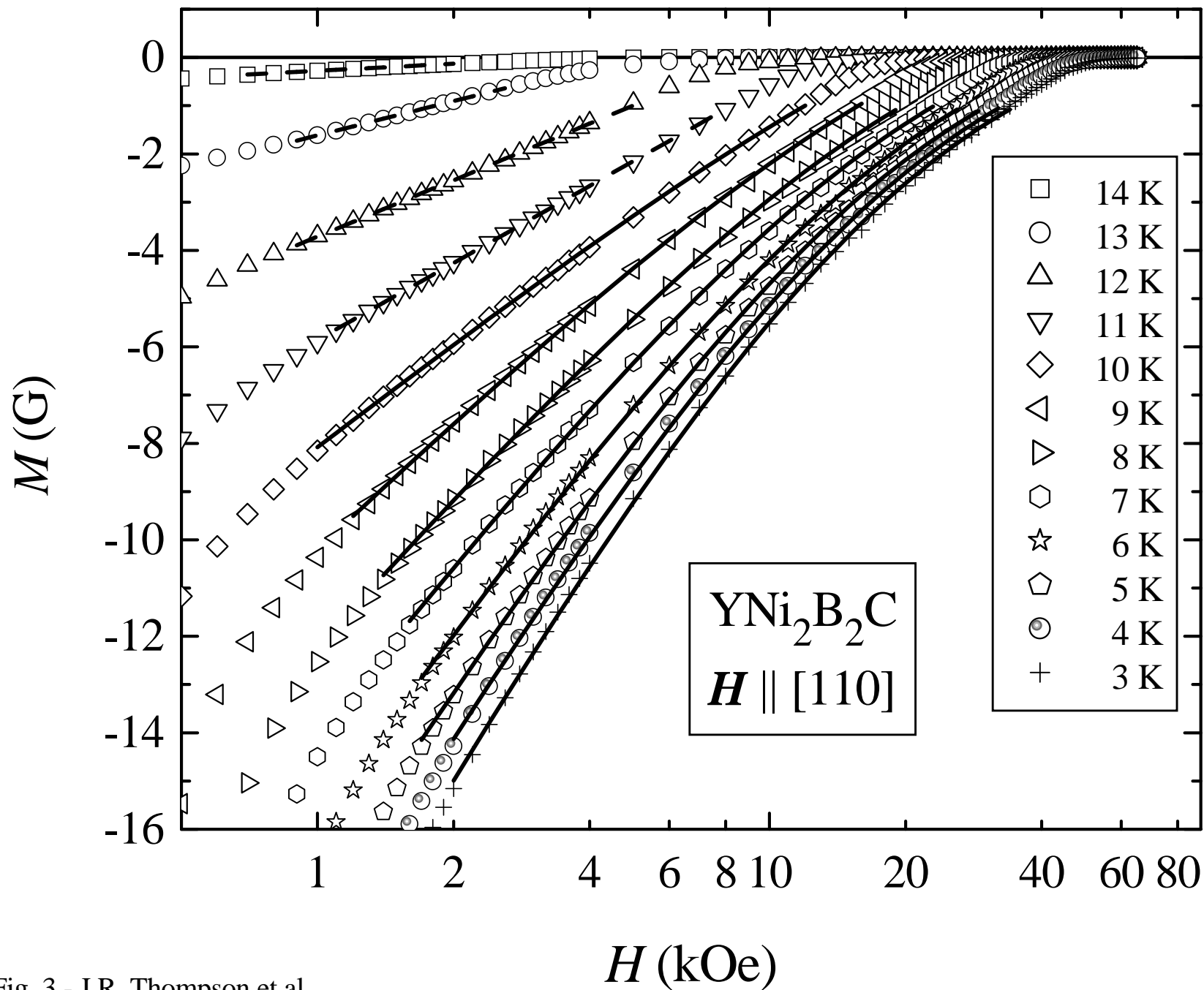


Fig. 3 - J.R. Thompson et al.

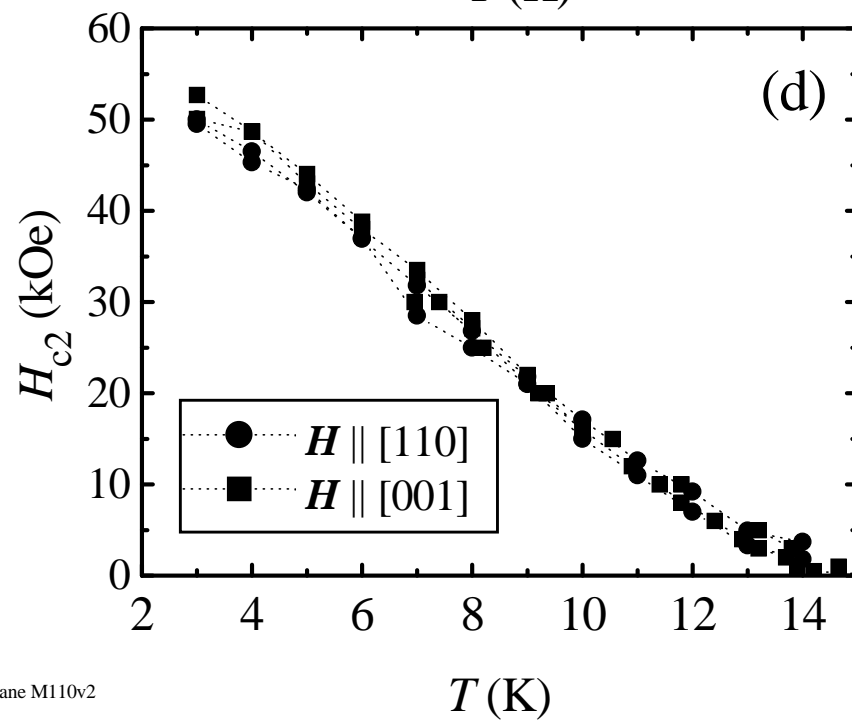
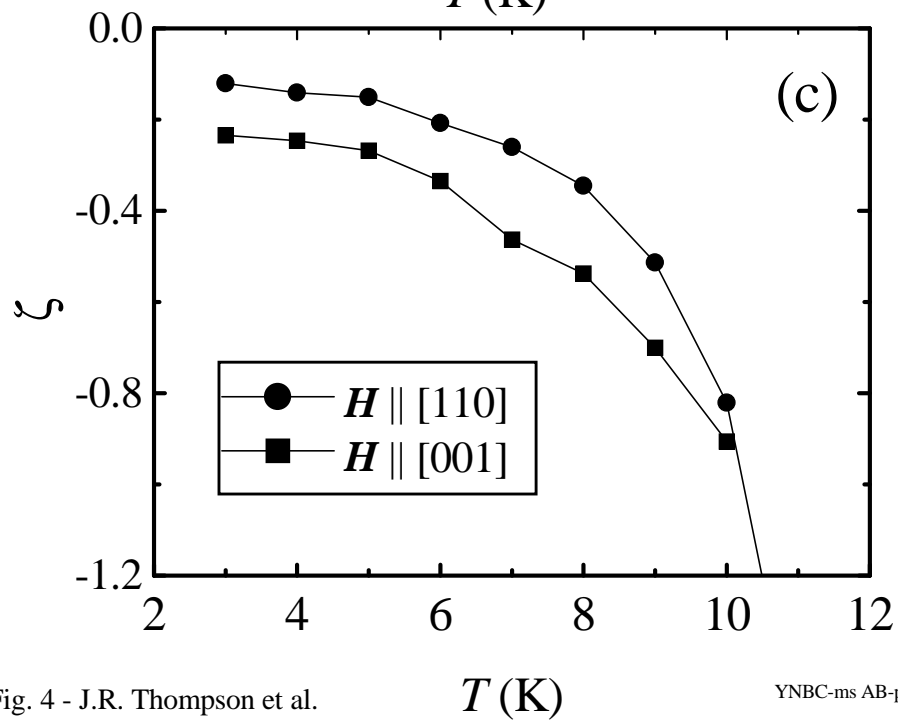
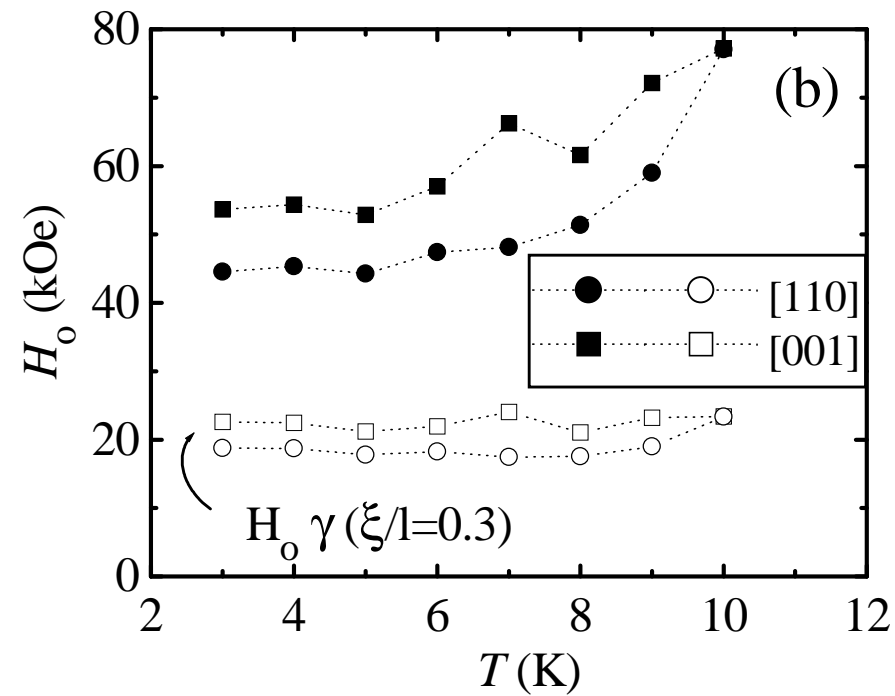
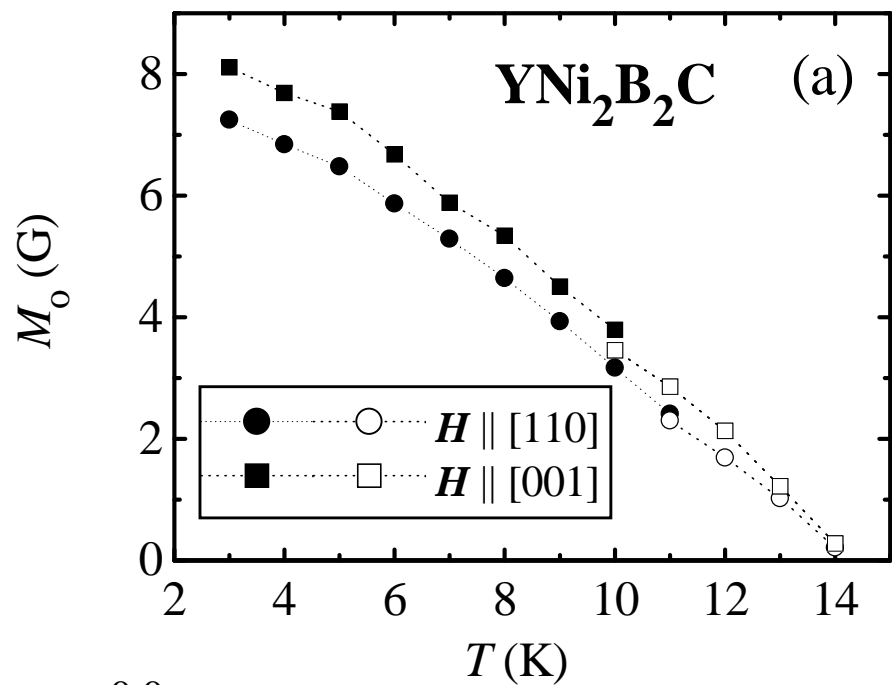


Fig. 4 - J.R. Thompson et al.

YNBC-ms AB-plane M110v2

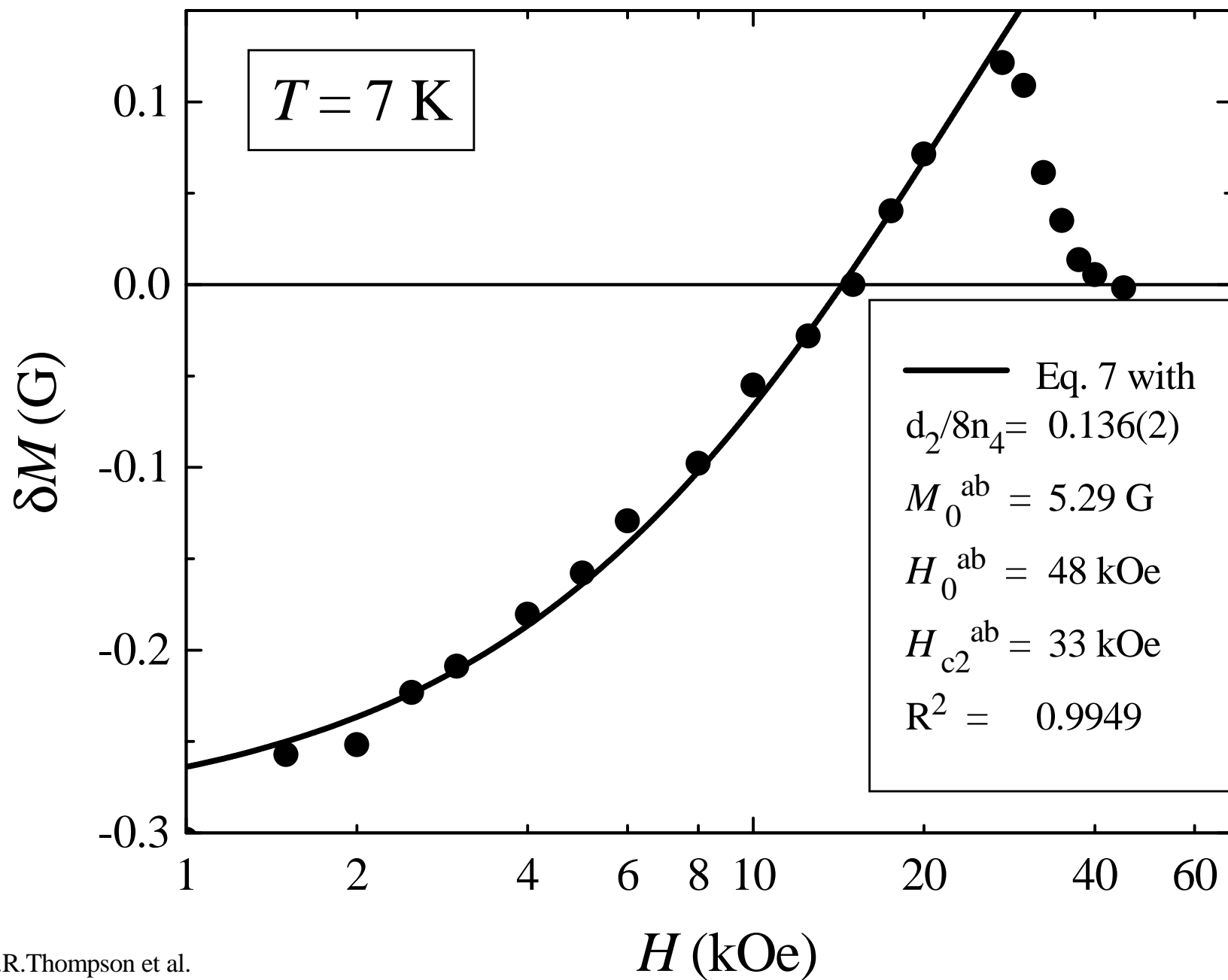


Fig. 5 - J.R.Thompson et al.